A first-principle study of $NaMPO_4$ (M = Mn, Fe, Co, Ni) possible novel structures as cathode materials for sodium-ion batteries: structural and electrochemical characterisation.

F. Bianchini,* H. Fjellvåg, and P. Vajeeston†

Centre for Materials Science and Nanotechnology

Department of Chemistry

University of Oslo, Box 1033 Blindern,

N-0315 Oslo, Norway

(Dated: August 3, 2018)

Abstract

Transition metal containing polyanion compounds are effective excellent electrode materials for sodium-ion batteries due to their high intrinsic electrochemical potentials and to the resulting high energy density. Iron sodium phosphates, in particular, are attractive due to the large natural abundance of both Na and Fe. These materials have been extensively studied in their most common olivine structures: maricite and triphylite. In this work, we expand the current knowledge of this class of materials by investigating the structural properties and the energetics of a series of modification exhibiting different coordination for the intermetallic atom M = Mn, Fe, Co, Ni by means of density functional theory calculations. An expanded-volume $NaFePO_4$ configuration with the zeolite ABW structure is predicted to be stable at high temperature. This type of structure, presenting a tetrahedral Fe–O coordination geometry, has been previously reported only for the $NaCoPO_4$ case. A semi-amorphous phase is predicted to be a possible metastable intermediate configuration between the known octahedral coordinated structures and the novel tetrahedral-coordinated one. The electrochemical characterisation of the latter reveals a similar equilibrium voltage as triphylite, and a larger diffusion barrier caused by the incompressibility of the PO_4 tetrahedra along the diffusive path. This result offers important insight about the correlation between the diffusive properties of ions and their local chemical environment.

PACS numbers: 61.59.Ah, 61.72.jd. 66.30.Fq, 82.45.Fk

* http://www.mn.uio.no/kjemi/english/people/aca/fredebi/; federico.bianchini@smn.uio.no

† http://folk.uio.no/ponniahv

I. INTRODUCTION

In recent years sodium-ion batteries (SIB) are attracting increasing interest from the scientific community due to the widespread abundance of sodium and its consequently low cost. They are considered the most attractive and cost-effective alternative to lithium-ion batteries (LIB), due to the chemical similarities between Li and Na ions, which would facilitate the conversion between battery technologies. From the perspective of atomistic *ab initio* simulations, a great interest has been shown by the community in investigating the structural properties and the ionic mobility of several novel electrode candidates, including layered oxides, titanates and phosphates [1–3]. The family of sodium iron phosphate $NaFePO_4$, in particular, is attractive due to the large abundance of both Fe and Na and has been the object of many recent investigations [4–10]. Notably, $NaMPO_4$ compounds exhibit a different polymorphism with respect to their Li-based counterparts. Maricite $NaFePO_4$ (m-$NaFePO_4$) is a natural mineral, observed for the first time in high-temperature corrosion studies in the late 1970s [11] and later characterised by X-ray diffraction (XRD) [12]. This configuration presents an olivine structure (space group *Pmnb*) similar to its Li-based analogous. However, the occupation of Na and Fe sites is reversed, leading to a large separation (~ 4.4 Å) between Na atoms. Due to the resulting poor ionic conductivity, maricite is traditionally reported as electrochemically inactive [4, 13]. Notably, more recent works report electrochemical activity for this material, at the expenses of its structural stability. In Ref. 5, a phase transition is shown to occur after the first cycle, highlighted by a drop in capacity. Further cycling of the battery revealed a good capacity retainment for over 300 cycles. In a more recent study, the flattening of the XRD pattern is observed after the first desodiation, indicating amorphisation of the material [6]. The original XRD pattern is never recovered during electro-chemical testing, and the cathode is shown to retain 95% of its initial capacity after 200 cycles.

Triphylite $NaFePO_4$ (t-$NaFePO_4$) is commonly synthesised by ion exchange from a $LiFePO_4$ precursor. It thus presents the same ionic occupation of the latter, resulting in improved ionics. Triphylite is sometimes labelled as 'olivine' $NaFePO_4$ in the literature. This denomination is ambigous, as both m-$NaFePO_4$ and t-$NaFePO_4$ belong to the *Pmnb* (*No* 62) space group. The synthesis process via ion substitution from a t-$LiFePO_4$ precursor is shown to be effective for the first time in Ref. 7, and the so-obtained structure

is fully resolved by XRD analysis in Ref. 14. The complete sodiation of olivine $FePO_4$ is also found to be fully reversible and to occur in two steps, with the formation of an intermediate $Na_{0.7}FePO_4$ structure, not observed in the Li case. The stability of t-$NaFePO_4$ is investigated by thermal differential analysis, finding an irreversible transition to maricite at $\sim$ 480°C, with a correspondent volume shrinkage of the sample. The structure and the energetics of these modifications is also analysed by first-principle calculations based on density functional theory (DFT). The intercalation/deintercalation potential (equilibrium voltage) is calculated, finding values between 2.8 eV and 3.0 eV, smaller than the reported value of 3.5 eV for maricite [14]. Notably, t-$NaFePO_4$ can also be synthesised by topotactic reactions using solid-state synthesis in molten salts at low temperatures ($\sim$100 K) [15].

Numerous reports of the electro-chemical performances of triphylite can be found in the literature. In Ref. 4 a discharge capacity of 147 mA h g^{-1} is measured in the first cycle operating in the 2–3 eV range. The plateau is observed at 2.8 V, in agreement with theoretical predictions [14]. In a more recent report the electrochemical performance of carbon-coated t-$NaFePO_4$ is compared to $LiFePO_4$ [8]. The NaFePO4 cathode retains 90% of its initial capacity (100 mA h g^{-1}) over 100 cycles. However, a larger volume change upon cycling and an overall lower rate performance with respect to its Li-ion counterpart is reported. In Ref. 16, a high-performance $NaFePO_4$ cathode powder is produced, reporting capacities in the range of 100–125 mA h g^{-1} with 13% decay over 100 cycles. A high discharge capacity of 111 mAh g^{-1} along with 90% retention over 240 cycles is reported for carbon coated t-NaFePO4/C [9]. Polythiophene-wrapped triphylite is also reported to exhibit a high capacity (142 mA h g^{-1}) with 93% retention [10]. The temperature dependence of the structural and electro-chemical properties of $FePO_4$ is studied in Ref. 17. An amorphous phase is reported in the range 380°C–480°C, while at higher temperature the material crystallises to a trigonal phase corresponding to space group $P32_1$. These two phases exhibit different properties when tested as cathodes for Na-ion batteries. The amorphous phase transforms into a $NaFePO_4$ matrix containing simultaneously amorphous $NaPO_4$ and triphylite. This structure exhibits an initial capacity of 143.5 mA h g^{-1}, with 70% retention over 200 cycles, and a Na-ion diffusivity of 2.5×10^{-13} cm^2 s^{-1}. The trigonal $FePO_4$ phase transforms instead into m-$NaFePO_4$ and thus exhibits a worse electro-chemical performance.

While $NaFePO_4$ structures are only observed as olivine modifications, Co-based phosphates present a more complex polymorphism [18]. Four distinct phases have been reported in experimental studies. The α phase, originally observed in Ref. 19 and later labelled 'pink $NaCoPO_4$' in Ref. 20, is isostructural to maricite. The second modification, known as β or blue $NaCoPO_4$, is comprised by twinned crystals and belongs to either the space group $P6_1$ or $P6_5$ [19, 21]. It has been more recently reported as a high-temperature hexagonal phase in a study focussed on electrode materials for hybrid supercapacitors [22]. The third phase exhibits the same tetrahedral connections as zeolite ABW (space group $P2_1/n$) [23]. The fourth modification, known as red $NaCoPO_4$, crystallises into trigonal bipyramidal CoO_5 groups, connected with the PO_4 tetrahedra in the space group $P2_1/n$ (*No* 14) [24]. This composite was recently synthesised using a microwave-assisted process and tested as cathode material due to its high voltage (4.1–4.4 eV) [25]. The sample firstly delivered 35 mA hg^{-1}, and its capacity increased during the first 40 cycles to a maximum of 40 mA h g^{-1}. The phase transitions and the formation enthalpies between the different $NaCoPO_4$ phases are reported in Ref. 18. Red $NaCoPO_4$ is found to be metastable while α and β $NaCoPO_4$ are identified as stable at low and high temperature respectively. To our knowledge, no studies of triphylite $NaCoPO_4$ have been reported.

Experimental reports for $NaMnPO_4$ and $NaNiPO_4$ are not as numerous as for Fe and Co. Similarly to $NaFePO_4$, maricite and triphylite are the most commonly reported structures [26]. In Ref. 27, novel synthesis methods for both these olivine $NaMnPO_4$ modifications are reported, based on the formation of suitable precursors that are easily transformed to target material by thermal decomposition (maricite) or by ion exchange (triphylite) reactions. As opposed to $NaFePO_4$, the precursor is a $KMnPO_4{\cdot}H_2O$ compound with a dittmarite-type structure. It is interested to note that, together with maricite and triphylite, a third phase is observed for Na–Mn based phosphates, natrophilite, which exhibits 50% occupation of the inequivalent cation sites by both Na and Mn [15]. In Ref. 22 m-Na$M$$PO_4$ (M = Ni, Co, Mn) is synthesised and tested as electrode for hybrid supercapacitors, finding a large capacitance in the case of $NaNiPO_4$, which can be further increased by coating with activated carbon. Structural studies for $NaNiPO_4$ confirm that this compound exist in two different forms, depending on the calcination temperature, 400° for triphylite and 550° for maricite [28].

TABLE I. List of the known NaMPO$_4$ polymorphs. The space group, the mineralogical name and the colour are indicated, as well as the labelling system used in this work.

Compound	space group	mineral. name	colour	references	label
m-NaFePO$_4$	$Pmnb$ (*No* 62)	maricite	–	[12]	octa/m 62
t-NaFePO$_4$	$Pmnb$ (*No* 62)	triphylite	–	[7]	octa/t 62
α-NaCoPO$_4$	$Pmnb$ (*No* 62)	–	pink	[19, 20]	octa/m 62
β-NaCoPO$_4$	$P6_1$,$P6_5$ (*No* 169, 170)	–	blue	[19, 21]	tetra/bp 62
NaCoPO$_4$	$P2_1/n$ (*No* 14)	–	–	[23]	tetra 14
NaCoPO$_4$	$P2_1/n$ (*No* 14)	–	red	[24]	bipyr 14
m-NaMnPO$_4$	$Pmnb$ (*No* 62)	maricite	–	[26, 27]	octa/m 62
t-NaMnPO$_4$	$Pmnb$ (*No* 62)	triphylite	–	[27]	octa/t 62
NaMnPO$_4$	$Pmnb$ (*No* 62)	natrophilite	–	[15]	–
m-NaNiPO$_4$	$Pmnb$ (*No* 62)	maricite	–	[22]	octa/m 62
t-NaNiPO$_4$	$Pmnb$ (*No* 62)	triphylite	–	[28]	octa/t 62

The polymorphism of NaMPO$_4$ is summarised in Table I, indicating space group, mineralogical name and colour. Only olivine structures are reported for Fe, Mn and Ni, named accordingly to the distinct site occupation of Na and M atoms. In the case of Co, modifications are labelled according to colour. The labels, reported in the last column of Table I, are introduced to identify each modification according to the coordination geometry of the MO_n group (octahedral, trigonal bipyramidal and tetrahedral) and to the space group. In the case of maricite and triphylite, a letter 'm' or 't' is introduced for clarity. We investigate here the configurational space of these phosphates by means of DFT modelling, with the aim of better understanding their polymorphism and of identifying possible novel structures which could be stabilised at particular pressure/temperature conditions. After a brief description of the theoretical methods (Sec. II), we analyse a variety of structures belonging to distinct space groups and exhibiting different coordination geometries for the MO_n group (Sec. III). We then proceed with the electro-chemical characterisation of NaFePO$_4$ compounds, focussing on the local minima of the energy curve (Sec. IV). We discuss the equilibrium voltages and the volumetric changes upon cycling, as well as the activation energy for Na diffusion in the considered structures, presented in Sec. V.

II. COMPUTATIONAL DETAILS

Density functional theory calculations are performed using the projected-augmented plane-wave (PAW) implementation of the Vienna Ab initio Simulation Package (VASP) [29–32]. The Perdew, Burke, and Ernzerhof (PBE) functional [33] is used for the exchange-correlation term. The Hubbard parameter correction (DFT+U) is included, following the rotationally invariant form [34]. Effective U values for the d states are chosen to be 4.0 eV (Fe, Mn) and 5.1 eV (Co, Ni), and the effective on-site exchange interaction parameter J is fixed to 1 eV. The optimised structures are obtained by minimising both the stress tensor and the Hellman-Feynman forces, using the conjugate-gradient algorithm with an energy convergence threshold of 10^{-3} eV. Brillouin zone (BZ) integration is performed with Γ-centred Monkhorst-Pack grids [35]. The electronic smearing is included following the Methfessel-Paxton scheme [36], using a gaussian broadening of 0.2 eV. The size of reciprocal-space grids varies with the shape and the volume of the simulation cell. It is found that a energy convergence within 20 meV is obtained using a **k**-points resolution of 0.15 Å^{-1} and a 500 eV kinetic energy cutoff for the plane wave expansion. For each of the considered modifications, a complete structural optimisation (cell shape and volume, atomic positions) is performed. The energy-volume curve is then obtained by calculations at fixed cell after applying a diagonal strain. Three 1% increments are used in both tension and compression, and the results are fitted to the Murnaghan equation of state [37]. Both ferromagnetic (FM) and anti-ferromagnetic (AFM) calculations are carried out for $NaFePO_4$ maricite, finding a total energy difference below 20 meV, comparable to the typical accuracy of a DFT calculation. Moreover, the magnetic moment for a Fe atom, as calculated from site-projection of d orbitals, is found to be 3.73 μ_B for both FM and AFM systems. In the rest of the paper only high-spin states are considered. Our result are also tested for varying values of U between 4 eV and 6 eV for both olivine and maricite $NaFePO_4$. The energy difference between these two phases shows variations up to 20 meV, compatible with the typical accuracy limit of DFT. Moreover, the equilibrium volumes are not significantly affected by varying the U parameter.

The formation energy E_f of Na-deficient compositions $Na_{1-x}FePO_4$ is calculated, following Ref. 38, as

$$E_f(1-x) = E(1-x) - (1-x)E(1) - xE(0) \tag{1}$$

where $E(x)$ indicates total energies as calculated with DFT, and $E(1)$, $E(0)$ are the reference energies for the fully lithiated and delithiated structures. The formation energy of these configurations is zero by construction. The formation energies of all the thermodynamically stable phases lie on the convex hull of the composition/formation energy curve. These structures are used to evaluate the equilibrium volume change upon desodiation, and the equilibrium voltages, obtained from the relation

$$V(x_1, x_2) = \frac{E(x_2) - E(x_1) - (x_2 - x_1)\mu}{x_2 - x_1} \tag{2}$$

where x_1, x_2 are the number of Na atoms in the unit cell and $E(x)$ is the total energy. The chemical potential μ accounts for the different stoichiometry, and it fixed to the total energy of a bcc crystal. The sodiated system is used as a reference, following [39, 40]. The activation energies for the diffusion of Na atoms are calculated using the NEB method [41]. A supercell is used to ensure a large separation between repeated images, and five replicas of the system are created by linear interpolation between the initial and final states. A NEB calculation is firstly performed to obtain a guess of the minimum energy path (MEP) and, in particular, to identify the configuration closer to the saddle point. The calculation is then restarted, using the climb-image method [42], allowing that configuration to reach the saddle point, thus improving the accuracy of the calculated diffusion barrier. The ionic optimisation steps for the intermediate images are carried out using the FIRE algorithm [43] with a force convergence threshold of 50 meV/Å. After convergence, the calculation is once again restarted, allowing for the relaxation of the lattice degrees of freedom following the solid-state NEB approach [44].

The Atomic Simulation Environment (ASE) [45, 46] is used for converting format of input/output files and for data analysis. The ball-and-stick and the coordination polyhedral models are rendered using VESTA [47]. The data plots are displayed using gnuplot [48]. The space group symmetries of crystals are identified using the FINDSYM software [49]

III. STRUCTURAL STABILITY

In this section we present a study of the energetics and of the structural properties of a set of NaMPO$_4$ modifications. We selected an initial set of 30 candidates is from the ICSD database [50]. The complete list of these structures is reported in the Table S1 and S2, noting the ICSD Collection Code and the original chemical compositions. The energy difference with respect to maricite for the 12 most favourable structures is reported in Table II, together with the equilibrium volumes. The values for the bulk modulus and its derivative with respect to pressure, similarly obtained by fitting to the Murnaghan equation of state, are reported in the Table S5. The energy-volume curves are displayed in Fig. 1 for NaFePO$_4$ and NaCoPO$_4$. Equivalent plots for the case of Mn and Ni can be found in Fig. S1. The reported structures are labelled accordingly to the space group number and to the coordination geometry of the MO_n group. A correlation between this feature and the equilibrium volumes is observed.

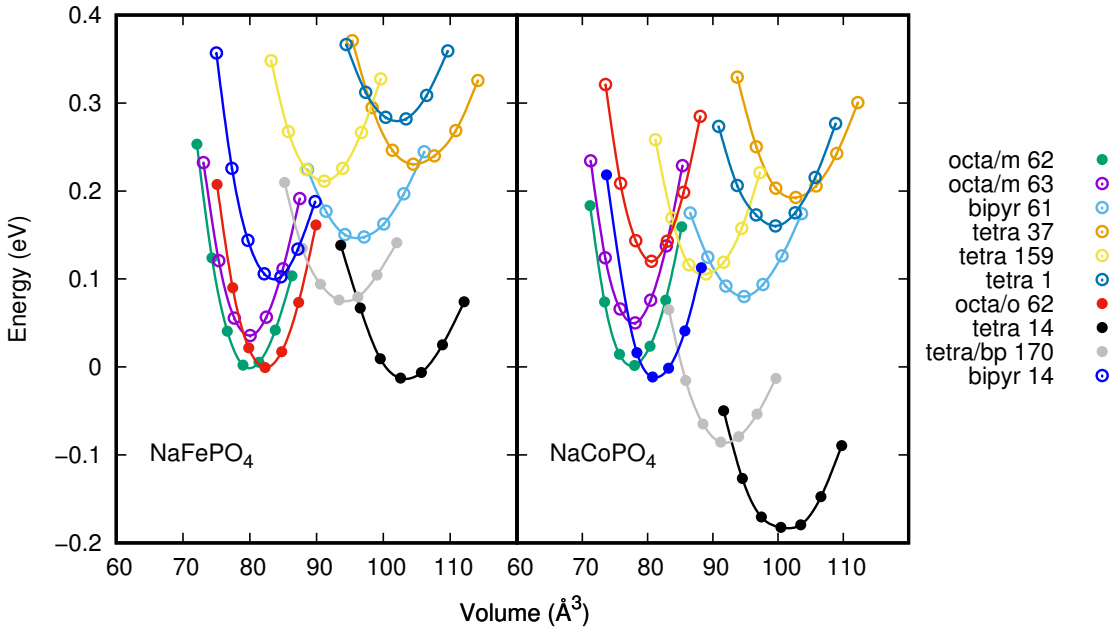

FIG. 1. Energy-Volume curve for NaFePO$_4$ and NaCoPO$_4$ modifications, labelled according to the space group and to the coordination geometry of the MO_n group (octahedral 'octa', tetrahedral 'tetra', trigonal bipyramidal 'bipyr' or a mixture of the last two 'tetra/bp'). The letters 't' and 'm' indicate triphylite and maricite respectively. The total energy of the latter is used as reference. Filled symbols indicate local minima of the system.

TABLE II. Equilibrium energy and volumes per formula unit as obtained from fitting to the Murnaghan equation of state for the analysed $NaMPO_4$ (M = Mn, Fe, Co, Mn) modifications. The total energy of maricite is used as reference. Structures are labelled according to the coordination of the M atom (octahedral 'octa', tetrahedral 'tetra', trigonal bipyramidal 'bipyr' or a mixture of the last two 'tetra/bp'). The letters 'm' and 't' indicate maricite and triphylite respectively.

sp. gr.	coor.	Mn		Fe		Co		Ni	
		V (Å^3)	E (eV)	V (Å^3)	E (eV)	V (Å^3)	E (eV)	V (Å^3)	E (eV)
62	octa/m	80.85	0.00	78.98	0.00	78.00	0.00	75.29	0.00
62	octa/t	85.83	-0.11	82.28	0.00	80.59	0.10	78.69	0.01
33	octa/t	85.84	-0.11	82.27	0.00	81.10	0.12	77.71	0.01
19	octa/t	85.25	-0.11	81.85	0.01	80.29	0.10	77.88	0.01
63	octa/m	81.04	0.01	80.06	0.04	78.10	0.05	75.04	0.06
170	tetra/bp	96.62	0.07	93.35	0.08	91.20	0.00	91.46	0.10
14	bipyr	85.98	0.01	82.16	0.11	80.77	-0.01	79.84	0.01
61	bipyr	97.94	0.26	97.12	0.15	94.80	0.08	100.30	0.39
159	tetra	94.24	0.26	91.15	0.21	88.97	0.10	87.29	0.30
14	tetra	106.27	-0.06	102.58	-0.01	100.43	-0.19	98.20	0.12
37	octa	108.99	0.38	104.46	0.23	102.71	0.19	99.83	0.31
1	tetra	104.44	0.28	100.34	0.29	99.59	0.16	98.91	0.37

The close-packed structures are characterised by smaller volumes and octahedral M–O coordination. We have identified 5 of these structures, including maricite and triphylite, labelled 'octa/m 62' and 'octa/t 62' respectively. The $BaNdGaO_4$ and the $NaCdPO_4$ structures (SG *No* 19 and *No* 33 respectively) relax to equilibrium configuration indistinguishable from 'octa/t 62', with perfectly overlapping energy-volume curves. The $LiFePO_4$ structure (SG *No* 63) relaxes to a maricite-like geometry, characterised by a smaller elementary cell (2 vs 4 formula units), resulting in equidistant neighbouring Na atoms (4 nearest neighbours, 4.54 Å separation). In maricite 2 inequivalent shells of 2 atoms each are present, at 4.40 Å and 4.63 Å. This asymmetry yields to an energy gain of 10 meV per formula unit without modifying the equilibrium volume. The 'octa/m 63' modification is therefore unstable, and can be obtained only at high pressure conditions.

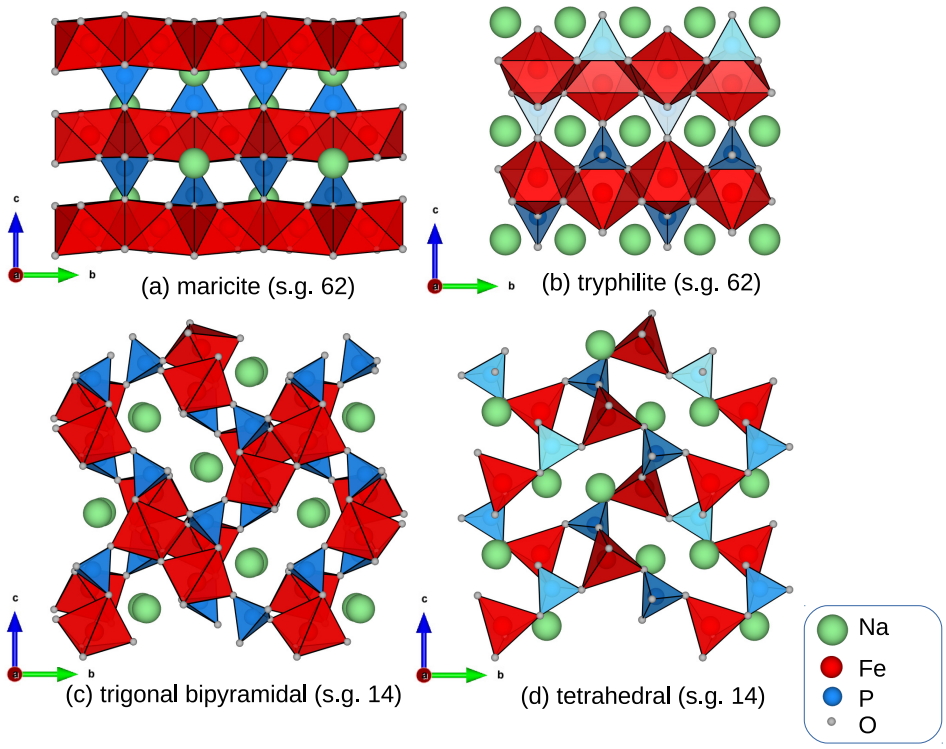

FIG. 2. Known NaMPO$_4$ modifications exhibiting different MO_n coordination group. The coordination geometry and the group numbers are indicated.

The equilibrium geometries of maricite and triphylite are displayed using coordination polyhedra in Fig. 2 in panels (a) and (b) respectively. As from Table II, these structures are found to be close in energy (within DFT accuracy), consistently with other theoretical reports. In Ref. 14, maricite is predicted to be favourable by 16 meV using DFT+U calculations. This energy difference is comparable with the changes in energy observed at the varying of the U parameter or of the initial sign of the magnetic moments for Fe atoms, as previously detailed in Sec. II. We also note that in the Mn case triphylite is more favourable than maricite. This is in qualitative agreement with the fact that a natrophilite-type phosphate is reported only in the case of NaMnPO$_4$ [15]. In Ref. 28, very accurate calculations are performed for the NaNiPO$_4$ system using the HSE06 hybrid functional. These calculations provide structural parameters closer to experimental data. The volume of the cell in particular is consistently smaller with respect to standard PBE calculations because of the stronger electron localization introduced by the Hartree-Fock exchange functional.

As the equilibrium volume is increased, the number of oxygen atoms neighbouring M decreases, and a MO_5 trigonal bipyramidal group is thus observed. Only one of the analysed modification presents a symmetrical coordination group ('bibyr 14', blue line in Fig. 1), with a calculated Fe–O bond length of 2.10 Å. This type of structure, shown in Fig. 2 with coordination polyhedra, is not energetically favourable in the case of $NaFePO_4$, but it is an experimentally observed as a metastable $NaCoPO_4$ modification [18, 24]. Further increasing of the equilibrium volume causes a deformation of the bipyramidal group, as observed in the configurations 'bipyr 61' and 'bipyr 14'. The latter shares both space group symmetry and coordination type with the previously described symmetric bipyramidal structure, exhibiting however different properties, as clear from Table II. Its energy-volume curve is not reported in Fig. 1 due to a significant overlap with the similar structure 'bipyr 61' (light blue curve). The length of the Na–O bonds is ~ 2 Å at the base of the pyramid and for one of the vertices. The other oxygen atom at the vertex is placed farther, at about 2.50 Å from the Fe atom. This geometry cannot be considered tetrahedral, as the Fe atom and the three O atoms at the base of the pyramid are coplanar. It indicates nevertheless that the bipyramidal group is not robust, and tetrahedral Na–O coordination is likely to arise at large volumes.

Within the structure labelled as 'tetra/bp 170', both tetrahedral MO_4 groups and distorted bipyramidal MO_5 configurations are observed. The typical Na–O distance for tetrahedral coordination is 2 Å, and the bipyramidal groups present similar features to the previously discussed geometry. This modification is reported as stable for the $NaCoPO_4$ system [18, 19, 22]. It is found here to be indeed energetically favourable in the intermediate volume range, not only for the Co-based system but also for Fe and Mn. This modification, displayed with coordination polyhedra in Fig. 4, is considerably different from the other structures considered in this work. It is characterised by a very large unit cell ($10.32 \times 10.32 \times 24.27$ Å^3, 24 formula unit) and by a general lack of local ordering. As reported in Table s4, 4 distinct M, Na and P sites can be identified, and 16 O sites. The M atoms form different coordination group with O, as already discussed, and so do the Na atoms, for which no regular polyhedron can be identified. For these reasons, this phase can be considered semi-amorphous. The fact that this is not energetically unfavourable is not an unexpected result, as non-crystalline $NaMPO_4$ structures are reported in literature in the 380–480° temperature range or as the result of the desodiation of maricite [6, 17].

For larger equilibrium volumes, a tetrahedral MO_4 coordination group is observed. Most of configurations of this type ('tetra 37', 'tetra 1', 'tetra 159') are found to be energetically unfavourable and they are not further analysed in this work. The 'tetra 14' modification (black line in Fig. 1), originally reported in an experimental work on $NaCoPO_4$ [23], is found instead to be a local high temperature minimum for all the considered M atoms. In the case of $NaFePO_4$, this structure is found to be as favourable as maricite, and it should be therefore possible to synthesise it, following e.g. a high temperature route. The equilibrium geometry is displayed in Fig. 2 with coordination polyhedra. The calculated Fe–O bond-length is 2 Å, as reported for the FeO_4 tetrahedral groups in the semi-amorphous modification.

In all the considered equilibrium structures, the P–O coordination geometry is tetrahedral, with equilibrium bond lengths of 1.55 Å for the octahedral-coordinated structures and 1.56 Å for the tetrahedral-coordinated ones. In the semi-amorphous structure, the tetrahedra can be either stretched or compressed, with P–O bond lengths varying between 1.52 Å and 1.58 Å. These bond-length variations, always below 3%, indicate a very robust covalent bonding between these atoms. This feature is desirable, as it improves the structural stability of the electrode. It can however affect the MEP of a diffusing Na ion and the associated activation energy, as we will illustrate in Section V.

As a final part of this section, we show the comparison between the experimental data reported in literature and the results of our calculations in Table III. The agreement is remarkably good (within 2% in most of the cases). In the case of Co-based maricite a discrepancy is observed between different experimental observation of the lattice parameter b. In Ref. 19, the value 7.78 Å is indicated, whereas both Ref. 20 and 18 report smaller values, around 6.80 Å. Our DFT calculations confirm the latter, as we obtain $b = 6.85$ Å as a result of geometric optimisation. We note that the our calculations tend to predict larger lattice parameters than the experimental results. This deviation is small, and can be corrected using hybrid functionals (e.g. HSE06), as shown in a recent work on nickel sodium phosphates [28].

TABLE III. Comparison with literature for the structural parameters of the considered NaMPO$_4$ (M = Mn, Fe, Co, Ni) modifications, labelled according to space group and coordination geometry.

M	modif.	source	a (Å)	b (Å)	c (Å)	β	V (Å^3/f.u.)
Mn	62 octa/m	ref. 22	9.085	6.905	5.115	90.00	80.22
Mn	62 octa/m	ref. 26	9.088	6.904	5.113	90.00	80.20
Mn	62 octa/m	ref. 27	9.072	6.909	5.118	90.00	80.20
Mn	62 octa/m	this work	9.174	6.904	5.106	90.00	80.85
Mn	62 octa/t	ref. 15	10.558	6.336	4.997	90.00	83.55
Mn	62 octa/t	ref. 27	10.528	6.321	4.985	90.00	82.92
Mn	62 octa/t	this work	10.670	6.406	5.023	90.00	85.82
Fe	62 octa/m	ref. 4	9.001	6.874	5.052	90.00	78.15
Fe	62 octa/m	ref. 12	8.990	6.862	5.047	90.00	77.82
Fe	62 octa/m	this work	9.082	6.867	5.065	90.00	78.97
Fe	62 octa/t	ref. 14	10.406	6.219	4.950	90.00	80.02
Fe	62 octa/t	ref. 15	10.421	6.212	4.953	90.00	80.02
Fe	62 octa/t	this work	10.495	6.229	5.002	90.00	82.27
Co	62 octa/m	ref. 19	8.871	7.780	5.023	90.00	75.52
Co	62 octa/m	ref. 20	8.896	6.800	5.034	90.00	76.12
Co	62 octa/m	ref. 18	8.878	6.795	5.029	90.00	75.85
Co	62 octa/m	this work	9.013	6.851	5.053	90.00	78.00
Co	170 tetra/bp	ref. 19	10.166	10.166	23.881	90.00	89.06
Co	170 tetra/bp	ref. 22	10.169	10.169	23.868	90.00	89.06
Co	169 tetra/bp	ref. 18	10.167	10.167	23.872	90.00	89.06
Co	170 tetra/bp	this work	10.258	10.258	24.018	90.00	91.20
Co	14 tetra	ref. 23	5.221	9.983	7.388	90.21	96.77
Co	14 tetra	this work	5.198	10.548	7.328	91.02	100.42
Co	14 bipyr	ref. 24	5.786	11.095	9.923	92.70	79.60
Co	14 bipyr	this work	5.827	11.092	9.997	92.60	80.76
Ni	62 octa/m	ref. 22	8.773	6.737	5.034	90.00	74.37
Ni	62 octa/m	this work	8.888	6.728	5.019	90.00	75.02

IV. EQUILIBRIUM VOLTAGES

In this section, we discuss the equilibrium voltages for a selection of the previously described structures, focussing on the technologically relevant case of $NaFePO_4$. The tetrahedral coordinated zeolite ABW structure, labelled 'tetra 14', is of particularly interest, as it is predicted to be as energetically favourable as maricite, and it has never been reported in experimental studies on $NaFePO_4$. The case of maricite is not investigated, as the cathode is known to lose its crystallinity after the first desodiation [6]. The equilibrium voltage of triphylite has been recently studied in DFT-based recent works [51, 52]. Contrarily to the case of $LiFePO_4$, in which all the intermediate configurations have positive formation energies, resulting in a flat convex hull connecting the fully lithiated structure to the fully delithiated one, Na_xFePO_4 presents several intermediate minimum. The most favourable one is observed in the 65-75% Na range (depending on the size of the model system), and correspond to the experimental superstructure reported in Ref. [53]. Other possible stable configurations are reported at 50% Na [51] or at 83% Na [52].

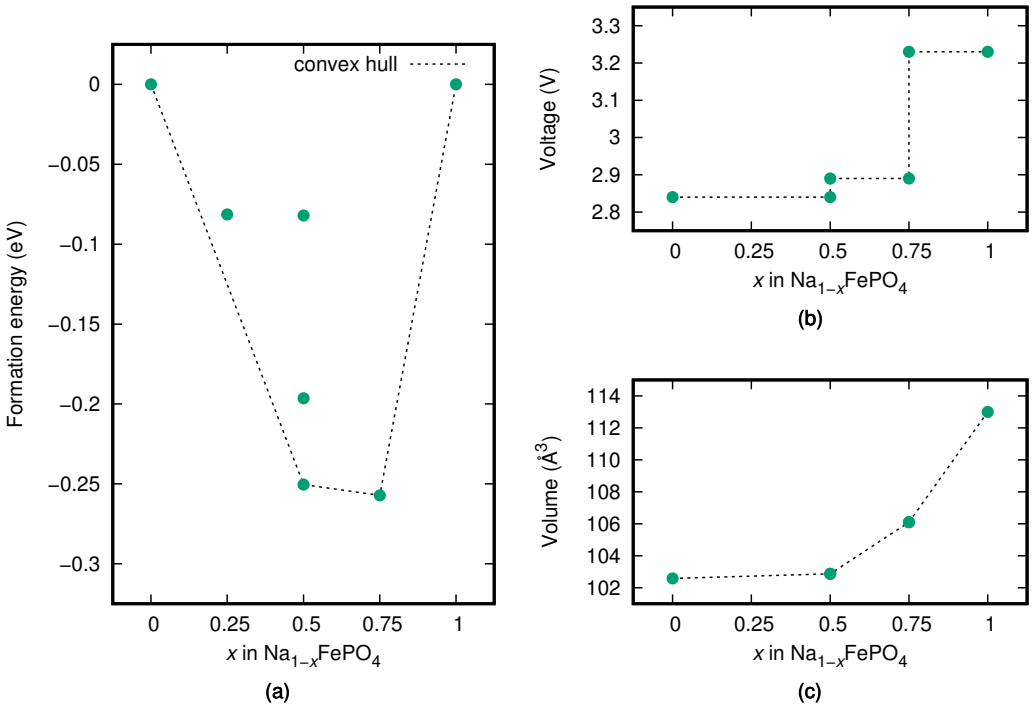

FIG. 3. Formation energy of Na-deficient configurations of the 'tetra 14' $NaFePO_4$ configurations (a). The equilibrium voltages (b) and the correspondent volumetric changes (c) are calculated for the points laying on the convex hull.

We report here a similar investigation for the 'tetra 14' structure. The formation energies of Na-deficient configurations are reported in Fig. 3 (a). A formation energy convex hull is constructed by connecting the low-energy configurations. We identify two stable intermediate configurations, at 50% and 25% Na. The presence of the latter indicates that the desodiation of this structure is different from the triphylite case, in which no stable configurations are observed in the low Na concentration range [51, 52]. The equilibrium voltage, calculated using these two minima and the fully sodiated/desodiated references, is shown in Fig. 3 (b). The first two transitions, from $NaFePO_4$ to $Na_{0.5}PO_4$ and then to $Na_{0.25}PO_4$, exhibit very similar potentials, 2.84 V and 2.89 V respectively, difficult to distinguish in experimental measurements. The last one, from $Na_{0.25}PO_4$ to the fully desodiated structure, has a 3.23 V potential. These values are similar to the reported ones for triphylite (2.89 V,2.92 V and 3.07 V), albeit the transitions are at different Na concentrations [52]. The volumetric change upon desodiation, calculated for the configurations laying on the convex energy hull, is reported in Fig. 3 (c). This change is negligible in the 0-50% range, but it increases rapidly as the structure gets progressively desodiated, reaching a 5% expansion at 25% Na and finally a 15% one in the fully desodiated configuration. Notably, triphylite exhibits the opposite trend upon desodiation, with a 5% volumetric contraction [52].

Finally, we discuss the desodiation of the semi-amorphous 'tetra/bp 170' modification. In this case, the construction of a convex hull is extremely demanding in terms of computational resources, due to the large size of the system (24 formula units in the elementary cell) and to the presence of 4 inequivalent Na sites. We also note that this phase is stable only at intermediate volumes between the energetically more favourable 'octa/t 62' and 'tetra 14' phases, and the volumetric change upon desodiation could be sufficient to destabilise it. We therefore decide to limit ourself to the high Na concentration regime, and to study only the energetics relative to desodiation of some specific cases. The equilibrium geometry of the 'tetra/bp' $NaFePO_4$ modification is displayed in Fig. 4 (a) using coordination polyhedra. The four inequivalent Na sites are indicated with different colours. For clarity, the sole Na network is shown in Fig. 4 (b), connecting nearest neighbours with sticks. We initially evaluate the potential associated to the deintercalation of a single Na atom from this structure. These values are found to be 2.55 eV, 2.98 eV, 3.01 eV and 3.30 eV for the sites Na1, Na2, Na3 and Na4 respectively, establishing deintercalation from the Na1 site as the most favourable process.

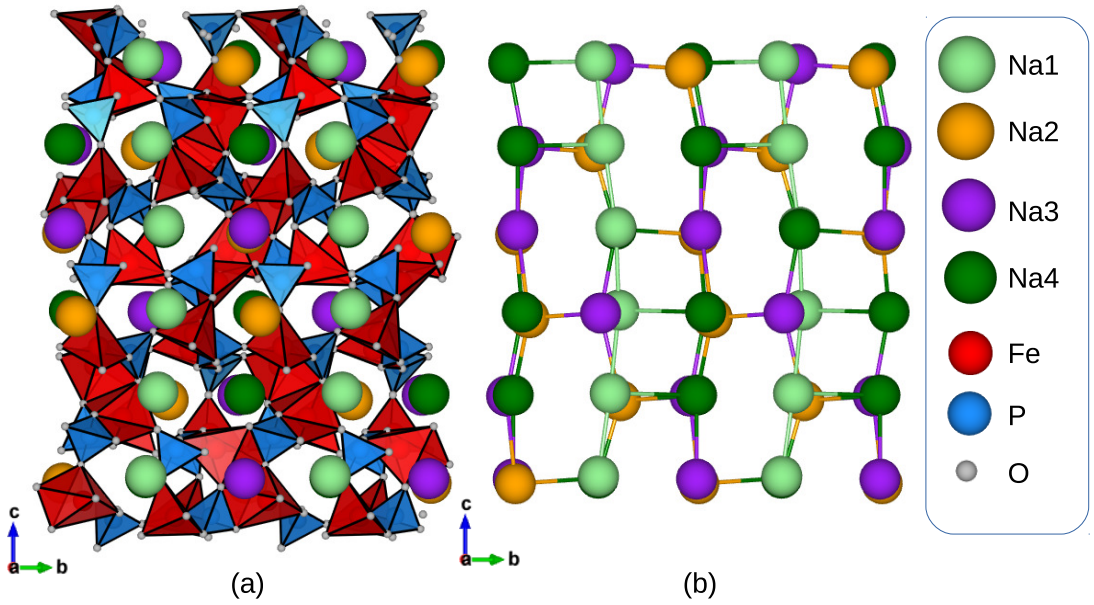

FIG. 4. Coordination polyhedra model of the tetra/bp 170 structure for $NaFePO_4$ (a). The Na network is highlighted in panel (b). Nearest neighbours atoms within a 5 Å cutoff are connected with sticks. Symmetrically inequivalent Na atoms are indicated using distinct colours.

Based on this result, we hypothesise that the desodiation of this structure starts with the deintercalation from the Na1 sites. To verify this, we perform a set of calculations at 75% Na concentration, removing 5 out of 6 atoms from Na1 sites, and a randomly chosen additional Na atom. The total energy of these structures is then compared to a reference structure in which Na1 sites have been fully depleted. While this set of calculations would not allow to determine the point laying at the convex energy hull, it can offer insight about the desodiation process, and disproof the previous hypothesis. The calculated energy differences are 4 meV, -199 meV and 310 eV for Na2, Na3 and Na4 respectively. These results indicate that deintercalation from the Na3 sites starts to occur before the Na1 channel is completely depleted, while deintercalation from Na4 remains an unfavourable event. In all these cases, a small volumetric expansion (0.6%) is observed. We argue that further desodiation of the structure could stabilise FeO_4 tetrahedra over the distorted bipyramidal groups, thus reconstructing the more favourable 'tetra 14' geometry.

V. IONIC DIFFUSIVITY

In this section, the diffusion of Na ions and the associated activation energies are discussed for the relevant $NaFePO_4$ structures. As a first step, the diffusion barriers are calculated for a single Na vacancy within the bulk of the experimentally known structures, maricite and triphylite. These structures exhibit very different diffusion properties, due to the site occupation of Na and Fe ions within the crystal. The activation energy for Na ion diffusion in maricite is calculated to be 1.70 eV. This value, compatible with the literature (see e.g. Ref. 6), indicates very poor electro-chemical performances. This prediction is, however, not directly comparable to the experiments, as desodiated maricite is not crystalline [6].

The triphylite matrix is instead stable upon Na cycling, and the diffusion process is reported to be similar to the analogous Li-ion case [8–10, 16, 17]. The trajectory of a diffusing Na ion, as obtained from a converged NEB calculation, is indicated in Fig. 5 (a) with a ball-and-stick model. The intermediate positions along the MEP are marked with green spheres, smaller than the one used for the initial and the final positions. The bond lengths at the saddle point between the Na ion and the nearest Fe and P atom are found to be 3.11 Å and 2.78 Å, compressed by 15% and 5% respectively with respect to the equilibrium references (3.64 Å and 2.92 Å). The diffusing ion follows a curved trajectory to reduce the interaction with the PO_4 tetrahedral group. The energy curve associated to this MEP is reported in Fig. 5(c). Its maximum, i.e. the activation barrier for Na diffusion, is found to be 0.37 eV, consistently with other theoretical predictions [51]. The diffusion of Na-ions within the novel 'tetra-14' $NaFePO_4$ structure is similarly investigated, reporting the MEP and the associated energy curve in Fig. 5 panels (b) and (d) respectively. Similarly to the olivine case, Na atoms diffuse along a 1-dimensional channel. Here, however, a percolating path is comprised by two inequivalent hops, as evident from the different size of the pores in the structure. The first hop has a small activation energy (0.10 eV). The second one, on the other hand, is characterised by a much larger barrier (0.55 eV) and by a linear diffusive trajectory. This is due to the path being comprised between two PO_4 tetrahedra, forcing the Na atom to equidistant positions to the P sites to minimise the repulsion. The Na–P bond length is 2.90 Å, 11% contracted with respect to the equilibrium value of 3.26 Å. This deformation, larger than the one observed in triphylite, is at the origin of the larger diffusion barrier, in spite of the larger equilibrium volume of the tetrahedral modification.

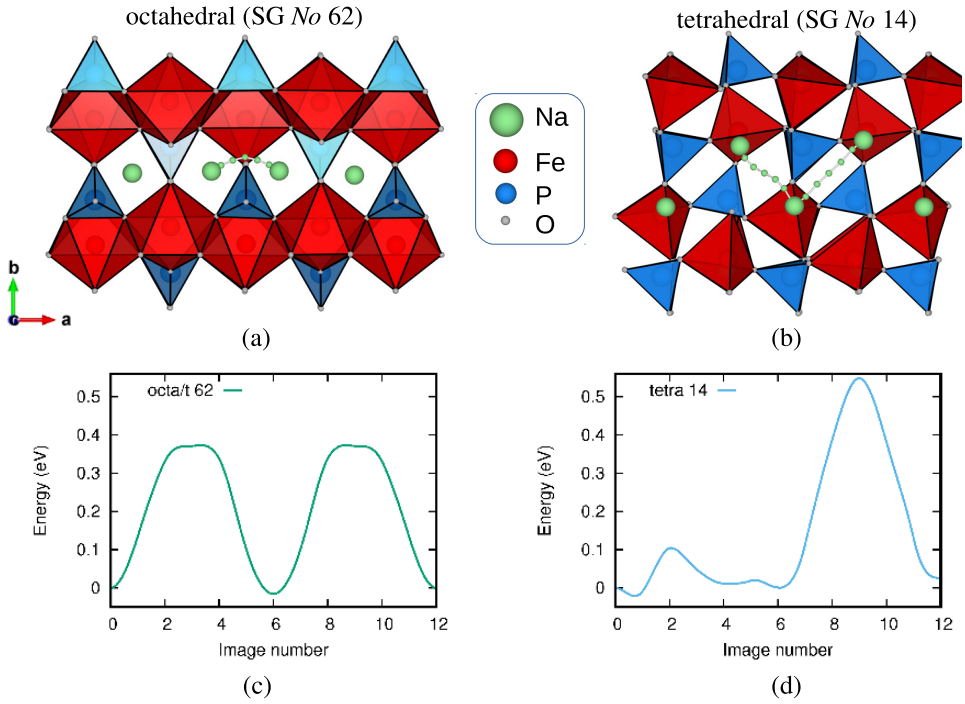

FIG. 5. Trajectory of a diffusive Na ion in the triphylite (a) and in the tetrahedral structure (b) and corresponding energy curves along the MEP (c,d).

To further understand the diffusion properties of Na atoms, we have calculated the activation energies for Na-deficient structures, focussing on the 25% sodium regime, at which the 'tetra-14' structure presents a point on the convex energy hull. For these desodiated configurations, the separation between neighbouring Na ions is 6.27 Å and 5.35 Å for the 'octa/t 62' and 'tetra 14' structures respectively. This distance is larger in the olivine phase because the two Na sites and the intermediate interstitial one are aligned, whereas in the tetrahedral case a zig-zag pattern of alternating filled and vacant Na sites is predicted. The first diffusing hop brings a Na atoms from its equilibrium position to the nearest interstitial site, following trajectories similar to the ones indicated in 5 (a,b). This hop is not connecting equivalent structural minima, as in the final configurations the Na ions present the same nearest neighbours distance as in the fully sodiated case. While this configuration does not belong to the convex hull, it needs to be accounted for while modelling ionic diffusion at the atomic scale. The energy difference between these configurations and the starting minima are found to be 0.73 eV and 0.26 eV for 'octa/t 62' and 'tetra 14' respectively, as can be observed from the energetics along the MEP reported in Fig. 6(a). Noteworthy,

an intermediate minimum is found along the MEP in the both cases (0.49 eV) From this configurations, it is reasonable to model the next event as the hop of a second Na atoms, the one neighbouring the previously considered one. This process repristinates the original distances between Na sites, but not the starting configurations, as these two atoms are no longer aligned with the remaining Na ions in the structure. The energy difference between these structures and the starting minima is 0.40 eV and 0.43 eV for 'octa/t 62' and 'tetra 14' respectively. Note that the energy cost is increased for the tetrahedral structure with respect to the second minimum, while the opposite trend is observed for the olivine system. This indicates that the interaction between these two atoms is stronger in the second case, as expected due to the alignment of lattice sites. Two more hops, similar to the ones previously described, are required to realigning the Na ions, thus closing the percolating path. In the olivine case, these two hops are equivalent two the previoly described ones due to the symmetry of the system. In the 'tetra 14' case this process is instead the two-atoms version of the second hop described in Fig. 5. The complete path, comprised of four hops, is schematised with ball-and-stick models in Fig. 6(b). The global activation energies for diffusion along these path are 1.06 eV and 0.78 eV for 'octa/t 62' and 'tetra 14' respectively. In both cases, this value is larger than the reference one obtained in the fully sodiated case, as clear from comparison with Fig. 5.

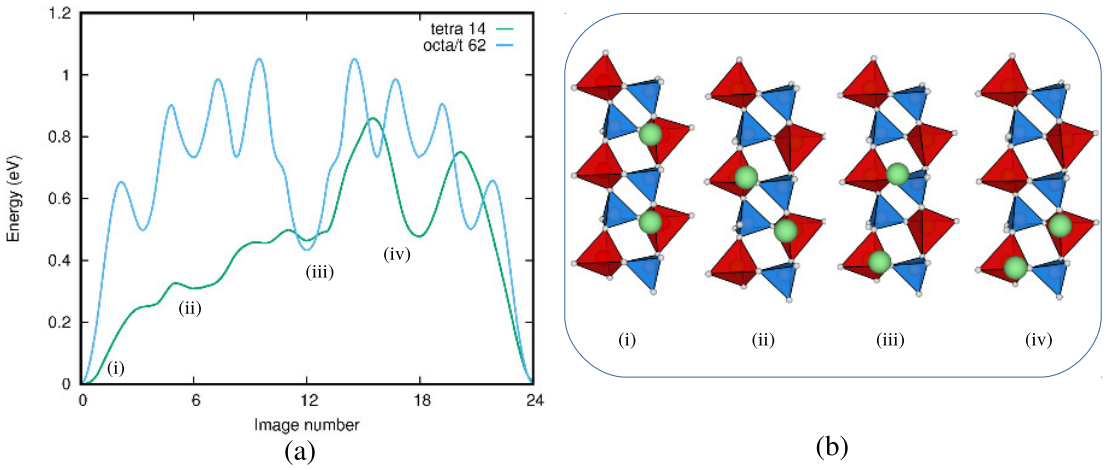

FIG. 6. Energy curve along the MEP for Na diffusion in triphylite and in the 'tetra 14' structure at the 25% Na concentration regime (a). Ball-and-stick model of the local minima encountered along the MEP in the 'tetra 14' case (b)

In the olivine case, the barrier is almost three times as large. This is the combined effect of the compressive strain due to desodiation and the energetics of the local minima encountered along the MEP. In the tetrahedral-coordinated structure, the activation energy for the desodiated phase is only 25% larger. While some of the intermediate minima are as unfavourable as in the olivine case, e.g the central point of the MEP in Fig. 6, the tensile strain observed in this case favours the diffusion of Na ions. These results indicate that the desodiation process presents distinct regimes characterised by different conductivity, and that the tetragonal coordinated structure might exhibit an improved capacity with respect to the olivine one at a given discharge rate, as the activation energies do not drastically change as the cathode is desodiated.

We now discuss the ionic diffusion properties of the semi-amorphous 'tetra/bp 170' $NaFePO_4$ modification. These are influenced by the distinct voltages for different Na sites, reported in the previous section. As already discussed, the desodiation of this structure starts with depletion of the Na1 sites. These sites are connected along a linear chain, as shown in Fig. 4, with an interatomic distance of 4.09 Å. The main ionic diffusive process at the initial stage of desodiation is therefore solely described by vacancy hopping in a straight line along the Na1 chain. The activation energy of this process is found to be 0.51 eV, comparable with the limiting step in the 'tetra 14' structure. When the Na1 channel is partially desodiated, other type of Na vacancies become energetically favourable, as previously discussed. The length of all the possible hops between neighbouring Na sites are summarised in Table IV. We note that alternative diffusion channels, not involving h1 steps, can follow either a Na2–Na3–Na2 pathway (the two hops involved are not equivalent, as from Table IV) or a Na2–Na4–Na2 one. These are shown in Fig. 7 (a) with a ball-and-stick model.

TABLE IV. Length of the possible hops between neighbouring Na sites in the semi-amorphous 'tetra/bp 170' $NaFePO_4$ modification.

$d_{\text{Na–Na}}$	Na1	Na2	Na3	Na4
Na1	4.09 Å	5.01 Å, 5.38 Å	5.09 Å, 5.39 Å	4.88 Å, 5.45 Å
Na2	5.01 Å, 5.38 Å	9.24 Å	3.99 Å, 4.38 Å	3.93 Å, 4.49 Å
Na3	5.09 Å, 5.39 Å	3.99 Å, 4.38 Å	6.32 Å	4.19 Å, 4.61 Å
Na4	4.88 Å, 5.45 Å	3.93 Å, 4.49 Å	4.19 Å, 4.61 Å	6.47 Å

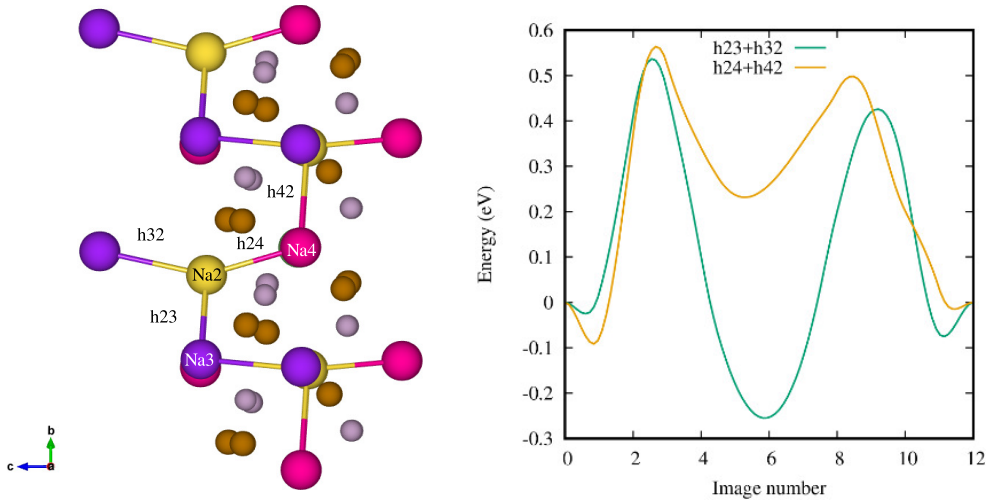

(a) (b)

FIG. 7. Diffusive pathways for Na ions in the 'tetra/bp 170' structure (a) and associated energetics along the MEP (b). For clarity, only a portion of the full structure is shown.

The activation energy for these processes is calculated, finding the values of 0.69 eV, 0.59 eV for Na2–Na3–Na2 and 0.65 eV 0.51 eV for Na2–Na4–Na2. The energy curve along the MEP is reported in Fig. 7. Note that the activation energies for the two pathways is very similar, despite the large voltage deviation between the Na3 and the Na4 sites. Altogether, the 'P65' structure is characterised as a mediocre conductor of Na ions, with performances lower than triphylite and of the novel 'tetra 14' structure.

VI. CONCLUSIONS

The structural properties of Na_2MPO_4 (M = Mn, Fe, Co, Ni) phosphates are investigated by means of first-principle calculations based on Density Functional Theory, finding a correlation between the coordination of the M atom (octahedral, trigonal bipyramidal and octahedral) and the equilibrium volume of $NaMPO_4$ modifications. Some of the examined structures, experimentally observed for $NaCoPO_4$, are found to be stable also in the commercially relevant case of $NaFePO_4$. The first structure is semi-amorphous and presents both distorted trigonal bipyramidal and tetrahedral coordination of Fe atoms. The second one, predicted to be particularly stable at high temperature due to its large equilibrium volume, exhibits tetrahedral PO_4 and FeO_4 coordination groups. We have calculated the equilibrium voltage for this phase, and reported the stable Na-deficient configurations as

obtained from the construction of the convex energy hull. We have investigated the diffusive paths and activation energies of Na atoms within these structures, and compared them with the known cases of maricite and triphylite. The semi-amorphous structure is found to have 4 non-equivalent Na sites, exhibiting different voltages. The most favourable sites for vacancy formation are connected along a 1-dimensional chain, along which diffusion can occur with a relative low migration barrier (0.51 eV). Other diffusion pathways in this structure involve larger activation energies. Ionic diffusion within the tetrahedral structure follows a zigzag path comprised of two steps. The second hop is found to be the bottleneck, due to the presence of two two PO_4 tetrahedra equidistant intermediate Na positions along the MEP. As a result of this symmetry, the shape of the MEP cannot deviate from a lines shape, as it does in triphylite to minimise the interaction with the PO_4 groups. Interestingly, diffusion barriers calculated at low Na concentration (25%) reveal a faster diffusivity in this tetrahedral-coordinated structure with respect to triphylite due to the tensile strength observed in the former due to desodiation.

ACKNOWLEDGMENTS

The authors gratefully acknowledge the Research Council of Norway (Grant agreement no. SELiNaB-255441) for financial support and for providing the computer time (project number NN2875k) at the Norwegian supercomputer facility.

[1] C. W. Mason, I. Gocheva, H. E. Hoster, and D. Y. W. Yu, Chem. Commun. **50**, 2249 (2014).

[2] A. Rudola, K. Saravanan, C. W. Mason, and P. Balaya, J. Mater. Chem. A **1**, 2653 (2013).

[3] S. M. Wood, C. Eames, E. Kendrick, and M. S. Islam, J. Phys. Chem. C **119**, 15935 (2015).

[4] K. Zaghib, J. Trottier, P. Hovington, F. Brochu, A. Guerfi, A. Mauger, and C. M. Julien, J. Power Sources **196**, 9612 (2011).

[5] A. Sun and A. Manivannan, ECS Transactions **35**, 3 (2011).

[6] J. Kim, D. H. Seo, H. Kim, I. Park, J. K. Yoo, S. K. Jung, Y. U. Park, W. A. Goddard III, and K. Kang, Energy Environ. Sci. **8**, 540 (2015).

[7] C. M. Burba and R. Frech, Spectrochimica Acta **65**, 44 (2006).

[8] Y. Zhu, Y. Xu, Y. Liu, C. Luo, and C. Wang, Nanoscale **5**, 780 (2013).

[9] Y. Fang, Q. Liu, L. Xiao, X. Ai, H. Yang, and Y. Cao, ACS Appl. Mater. Interfaces **7**, 17977 (2015).

[10] G. Ali, J. Lee, D. Susanto, S. Choi, B. W. Cho, K. W. Nam, and K. Y. Chung, ACS Appl. Mater. Interfaces **8**, 4 (2016).

[11] D. Broadbent, G. G. Lewis, and E. A. M. Wetton, "The chemistry of high temperature phosphate solutions in relation to steam generation," in *Water chemistry of nucler reactor systems* (1978) pp. 53–62.

[12] J. N. Bridson, S. E. Quinlan, and P. R. Tremaine, Chem. Mater. **10**, 763 (1998).

[13] B. L. Ellis, W. R. M. Makahnouk, Y. Makimura, K. Toghill, and L. F. Nazar, Nat. Mater. **6**, 749 (2007).

[14] P. Moreau, D. Guyomard, J. Gaubicher, and F. Boucher, Chem. Mater. **22**, 4126 (2010).

[15] K. T. Lee, T. N. Ramesh, F. Nan, G. Botton, and L. F. Nazar, Chem. Mater. **23**, 3593 (2011).

[16] N. Wongittharom, T. C. Lee, C. H. Wang, Y. C. Wang, and J. K. Chang, J. Mater. Chem. A **2**, 5655 (2014).

[17] Y. Liu, Y. Zhou, J. Zhang, S. Zhang, and P. Ren, J. Power Sources **314**, 1 (2016).

[18] S. N. Le, H. W. Eng, and A. Navrotsky, J. Solid State Chem. **179**, 3731 (2006).

[19] R. Hammond and J. Barbier, Acta Crystallogr. Sect. B **52**, 440 (1996).

[20] P. Feng, X. Bu, and G. D. Stucky, J. Solid State Chem. **131**, 160 (1997).

[21] P. Feng, X. Bu, S. H. Tolbert, and G. D. Stucky, J. Am. Chem. Soc. **119**, 2497 (1997).

[22] B. Senthilkumar, K. V. Sankar, L. Vasylechko, Y. S. Lee, and R. K. Selvan, RSC Adv. **4**, 53192 (2014).

[23] A. M. Chippindale, A. R. Cowley, J. Chen, Q. Gao, and R. Xu, Acta Crystallogr. Sect. C **55**, 845 (1999).

[24] P. Feng, X. Bu, and G. D. Stucky, J. Solid State Chem. **129**, 328 (1997).

[25] A. Gutierrez, S. Kim, T. T. Fister, and C. S. Johnson, ACS Applied Materials and Interfaces **9**, 4391 (2017).

[26] J. Moring and E. Kostiner, J. Solid State Chem. **383**, 379 (1986).

[27] V. Koleva, T. Boyadzhieva, E. Zhecheva, D. Nihtianova, S. Simova, G. Tyuliev, and R. Stoyanova, Cryst. Eng. Comm. **15**, 9080 (2013).

[28] M. Minakshi, D. Mitchell, R. Jones, F. Alenazey, T. Watcharatharapong, S. Chakraborty, and R. Ahuja, Nanoscale **8**, 11291 (2016).

[29] G. Kresse and J. Hafner, Phys. Rev. B **47**, 558 (1993).

[30] G. Kresse and J. Furthmüller, Comput. Mater. Sci. **6**, 15 (1996).

[31] G. Kresse and J. Furthmüller, Phys. Rev. B **54**, 11169 (1996).

[32] G. Kresse and D. Joubert, Phys. Rev. B **59**, 1758 (1999).

[33] J. P. Perdew, K. Burke, and M. Ernzerhof, Phys. Rev. Lett. **77**, 3865 (1996).

[34] A. I. Liechtenstein, V. I. Anisimov, and J. Zaanen, Phys. Rev. B **52**, R5467 (1995).

[35] H. J. Monkhorst and J. D. Pack, Phys. Rev. B **13**, 5188 (1976).

[36] M. Methfessel and A. T. Paxton, Phys. Rev. B **40**, 3616 (1989).

[37] F. D. Murnaghan, Proc. Natl. Acad. Sci. **30**, 244 (1944).

[38] A. Urban, D.-H. Seo, and G. Ceder, npj Computational Materials **2**, 16002 (2016).

[39] F. Bianchini, H. Fjellvåg, and P. Vajeeston, Phys. Chem. Chem. Phys. **19**, 14462 (2017).

[40] P. Vajeeston and H. Fjellvag, RSC Adv. **7**, 16843 (2017).

[41] G. Henkelman and H. Jónsson, J. Chem. Phys. **113**, 9978 (2000).

[42] G. Henkelman, B. P. Uberuaga, and H. Jónsson, J. Chem. Phys. **113**, 9901 (2000).

[43] E. Bitzek, P. Koskinen, F. Gähler, M. Moseler, and P. Gumbsch, Phys. Rev. Lett. **97**, 170 (2006).

[44] D. Sheppard, P. Xiao, W. Chemelewski, D. D. Johnson, and G. Henkelman, J. Chem. Phys. **136**, 074103 (2012).

[45] S. R. Bahn and K. W. Jacobsen, Comput. Sci. Eng. **4**, 56 (2002).

[46] A. H. Larsen, J. J. Mortensen, J. Blomqvist, I. E. Castelli, R. Christensen, M. Duak, J. Friis, M. N. Groves, B. Hammer, C. Hargus, E. D. Hermes, P. C. Jennings, P. B. Jensen, J. Kermode, J. R. Kitchin, E. L. Kolsbjerg, J. Kubal, K. Kaasbjerg, S. Lysgaard, J. B. Maronsson, T. Maxson, T. Olsen, L. Pastewka, A. Peterson, C. Rostgaard, J. Schitz, O. Schütt, M. Strange, K. S. Thygesen, T. Vegge, L. Vilhelmsen, M. Walter, Z. Zeng, and K. W. Jacobsen, J. Phys. Condens. Matter **29**, 273002 (2017).

[47] K. Momma and F. Izumi, J. Appl. Crystallogr. **41**, 653 (2008).

[48] T. Williams, C. Kelley, *et al.*, "Gnuplot 4.6: an interactive plotting program," (2013).

[49] H. T. Stokes and D. M. Hatch, J. Appl. Crystallogr. **18**, 237 (2005).

[50] M. Hellenbrandt, Crystallogr. Rev. **10**, 17 (2004).

[51] M. Nakayama, S. Yamada, R. Jalem, and T. Kasuga, Solid State Ion. **286**, 40 (2016).

[52] A. Saracibar, J. Carrasco, D. Saurel, M. Galceran, B. Acebedo, H. Anne, M. Lepoitevin, T. Rojo, and M. Casas Cabanas, Phys. Chem. Chem. Phys. **18**, 13045 (2016).

[53] M. Galceran, V. Roddatis, B. Acebedo, R. Arenal, I. Peral, and T. Rojo, Chem. Mater. **26**, 3289 (2014).

A first-principle study of $NaMPO_4$ (M = Mn, Fe, Co, Ni) possible novel structures as cathode materials for sodium-ion batteries: structural and electrochemical characterisation. Electronic Supplementary Information (ESI)

F. Bianchini,* H. Fjellvåg, and P. Vajeeston†

Department of Chemistry

University of Oslo, Box 1033 Blindern,

N-0315 Oslo, Norway

(Dated: March 26, 2018)

* federico.bianchini@smn.uio.no

† http://folk.uio.no/ponniahv

I. STARTING DATABASE

In this section we report the initial set of 30 structures used to explore the configurational space of Na intermetallic phosphates. Only the configurations close in energy to maricite (within a 0.4 eV window) are analysed in the main text. The full initial set is provided in Table S1 and in Table S2, indicating each structure with the correspondent ICSD Collection Code and with the original chemical composition. The space group (name and number) are also provided for each configuration for the sake of clarity, together with the energy difference (per formula unit) with respect to maricite. Note that some of these structures (e.g. ICSD collection code 82752) have been included twice in the dataset. This is due to the fact the maricite and tryphilite are related to each other by a swap of crystal sites between the Na and the Fe ions, and both maricite-like and tryphilite-like structures have been examined here for relevant octahedral coordination of the Fe atom. The structures presenting this inversion of ion sites are indicated with a ^{i} symbol after the ICSD Collection Code in Tables S1, S2. A discussion about the energy ordering of the structures for NaMPO$_4$ (M = Mn, Fe, Co and Ni) is presented in the main text.

Table S1. Entries of the ICSD databased analysed for this study. The space group and the original formula of the compound are reported for clarity. The total energy difference per formula unit with respect to maricite is indicated. The suffice i indicates inversion of the original lattice sites for Fe and Na, in order to change to maricite-like to tryphilite-like geometries. The second part of the table can be found in the next page.

ICSD	composition	space group		Energy (eV)
10472	$BaCdSnS_4$	$Fdd2$	(No 43)	0.44
50950	$LiZnPO_4$	Cc	(No 9)	0.28
237852	$NaFePO_4$	$Pmna$	(No 62)	0.00
280175	$NaCoPO_4$	$P2_1/c$	(No 14)	-0.01
15836	$LiCuVO_4$	$Imma$	(No 74)	3.56
72484	$CaMgNiH_4$	$P2_13$	(No 198)	1.09
14048	$NaCdPO_4$	$Pna2_1$	(No 33)	0.00
50457	$TlCuPO_4$	$C2/c$	(No 15)	0.43

Table S2. Entries of the ICSD databased analysed for this study. The space group and the original formula of the compound are reported for clarity. The total energy difference per formula unit with respect to maricite is indicated. The suffice i indicates inversion of the original lattice sites for Fe and Na, in order to change to maricite-like to tryphilite-like geometries.

ICSD	composition	space group		Energy (eV)
28106	$LiBGeO_4$	$Fmm2$	(No 42)	0.68
85671	$FeNaPO_4$	$Pnma$	(No 62)	0.00
82752	$FeNaPO_4$	$Pnma$	(No 62)	0.00
82752^i	$FeNaPO_4$	$Pnma$	(No 62)	0.25
86792	$BaBeSiO_4$	Cm	(No 8)	0.59
27647	$CaAlBO_4$	$Ccc2$	(No 37)	0.23
186517	$LiFeSiO_4$	$P1$	(No 1)	0.29
14364	$LiNaSO_4$	$P31c$	(No 159)	0.21
603205	$KYbSiS_4$	$P2_1$	(No 4)	0.55
263111	$CdBi2O_4$	$I4_1/amd$	(No 141)	1.04
28107	$SrBAlO_4$	$Pccn$	(No 56)	2.98
2929	$LiAlSiO_4$	$P6_422$	(No 181)	0.66
97767	$FeLiPO_4$	$Cmcm$	(No 63)	0.04
97767^i	$FeLiPO_4$	$Cmcm$	(No 63)	0.32
35451	$BaNdGaO_4$	$P2_12_12$	(No 19)	0.01
30886	$KCuPO_4$	$Pbca$	(No 61)	0.15
9271	$NaBePO_4$	$P2_1/c$	(No 14)	0.42
84709	$NaCoPO_4$	$P2_1/c$	(No 14)	0.11
82753	$NaCoPO_4$	$P6_5$	(No 170)	0.08
415458	$KFePO_4$	$P2_1/c$	(No 14)	0.15
56291	$LiFePO_4$	$Pnma$	(No 62)	0.00
56291^i	$LiFePO_4$	$Pnma$	(No 62)	0.00

II. ENERGY-VOLUME CURVES

We present here the energy-colume curves for NaMPO$_4$ (M = Mn, Ni), excluded from the main text due to the strong similarities with case of M = Fe. With respect to this aforementioned case, we observe a larger energy spreading between favourable and unfavourable structures. Tryphilite is observed to be particularly favourable in the case of Mn, consistent with the existence of natrophilite, a structure which exhibits 50% occupation of the inequivalent cation sites by both Na and Mn. In the case of Co a Fe-like behaviour is observed, with a greater preference for low-volume structures. This is the only case for which the phase labelled as 'tetra 14' is least favourable than the semi-amorphous 'tetra/bp 170'. This particular tetrahedral structure is nevertheless the most favourable with respect to the other examined cases presenting the same kind of coordination for the Fe atom. Overall, these compounds are less likely to exhibit polymorphism than NaFePO$_4$, being limited to maricite and tryphilite structures. The behaviour of Co based phosphates, examined in the main text and matching relevant experimental measurements, is unique within the series as the blue, the tetraheral and the red phases are observed, while tryphilite is not favourable.

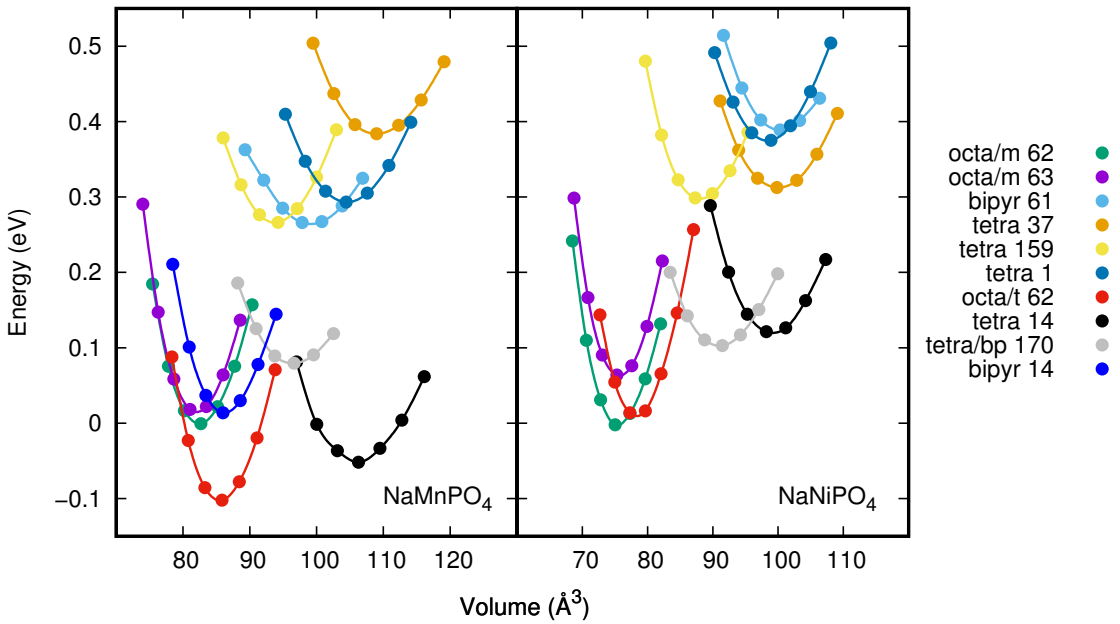

Fig. S1. Energy-volume curves per formula unit for the most energetically favourable configurations for NaMPO$_4$ (M = Mn, Ni) compounds. Energies (per formula unit) are reported using maricite as a reference. Structures are labelled according to the coordination of the M atom, octahedral ('octa'), tetrahedral ('tetra') trigonal bipyramidal ('bypir') or a mixture of the last two ('tetra/bp').

III. NOVEL STRUCTURES

We report here the equilibrium coordinates for the two energetically most favourable novel structures for $NaFePO_4$. The structure labelled as 'tetra 14' is reported in Table S3, and 'tetra/bp 170' in Table S4. The equilibrium volumes and the lattice parameters are reported in the main text, in respectively table I and II. The crystal symmetries of these systems are studied using the FINDSYM code, as referenced in the main text. The Wyckoff positions and the respective multiplicity are thus obtained and reported in Tables S3, S4. The parameters for the structural optimisation of these structures are reported in Section II in the main text.

Table S3. Equilibrium atomic coordinates for the 'tetra 14' $NaFePO_4$ structure.

Z	Wyckoff positions		x	y	z
Fe1	4	e	0.71997	0.34186	0.51712
Na1	4	e	0.22941	0.37052	0.01704
O1	4	e	0.04999	-0.03876	0.77051
O2	4	e	0.88109	0.33934	0.08923
O3	4	e	0.72136	0.67011	0.55922
O4	4	e	0.28696	0.62190	0.70455
P1	4	e	-0.01592	0.10348	0.77717

Table S4. Equilibrium atomic coordinates for the 'tetra/bp 170' $NaFePO_4$ structure.

Z	Wyckoff positions		x	y	z
Fe1	6	a	0.61115	0.82444	0.70964
Fe2	6	a	0.32662	0.65734	0.47971
Fe3	6	a	0.69396	0.86270	0.01823
Fe4	6	a	0.18700	0.88830	0.01155
Na1	6	a	0.06372	0.04718	0.09337
Na2	6	a	0.50063	-0.07221	0.24482
Na3	6	a	0.48756	0.45171	0.75409
Na4	6	a	0.53702	0.04931	0.08936
O1	6	a	0.55966	0.22676	0.15354
O2	6	a	-0.01316	0.79543	0.35206
O3	6	a	-0.00708	0.32075	0.04766
O4	6	a	0.75871	0.08438	0.25785
O5	6	a	0.64794	0.48636	0.85052
O6	6	a	0.07229	0.72902	0.14054
O7	6	a	0.59881	-0.08825	0.78246
O8	6	a	0.76940	0.26289	0.47704
O9	6	a	0.14424	-0.02721	0.84606
O10	6	a	0.29220	0.25519	-0.07872
O11	6	a	0.85851	0.06931	-0.00339
O12	6	a	0.35917	0.61369	0.73735
O13	6	a	0.19222	0.45538	0.51582
O14	6	a	0.51352	0.71795	0.85838
O15	6	a	0.71534	0.70992	-0.02941
O16	6	a	0.51626	0.64918	0.49817
P1	6	a	0.14806	0.31193	0.48102
P2	6	a	0.63450	0.32997	0.84626
P3	6	a	0.12973	0.77558	0.50502
P4	6	a	0.21683	0.88450	0.14520

IV. BULK MODULUS

We report here the bulk modulus and its derivative with respect to pressure for the examined structures, as obtained from fitting to the Murnaghan equation of state of energy-volumes curves, as specified in Section II in the main text. The values obtained for the 12 most favourable configurations for varying M = Mn, Fe, Co and Ni, are reported in Table S5, and complement the information presented in the main text (Table I).

Similarly to what observed for the equilibrium volume, the bulk modulus of these structures is correlated to the coordination of the M atom. The values reported for the octahedral phases (maricite, tryphilite and related structures) are significantly larger than what observed for expanded volume configurations. These values range from 80 to 100 GPa, following the ordering Ni > Co > Fe ≈ Mn and ehxibiting a negligible difference between triphylite and maricite.

Table S5. Bulk modukus and its derivative with respect to pressure for the $NaMPO_4$ series. Values are reported for all the structure with total energy per formula unit within 0.4 eV from maricite.

sp. gr.	coor.	Mn		Fe		Co		Ni	
		B (GPa)	B'	B (GPa)	B'	B (GPa)	B'	B (GPa)	B'
62	octa/m	81.34	5.80	80.87	5.43	86.38	6.23	92.80	6.29
62	octa/t	83.46	4.91	81.24	5.52	87.94	4.44	96.85	5.14
33	octa/t	83.79	4.75	88.11	4.41	88.41	4.70	97.79	4.30
19	octa/t	82.32	4.65	86.00	4.24	87.24	4.12	97.28	4.25
63	octa/m	88.36	5.32	85.57	5.56	92.28	4.99	98.73	4.99
170	tetra/bp	38.80	5.16	39.01	6.95	44.48	6.57	41.88	5.26
14	bipyr	72.28	6.32	71.69	6.21	81.70	6.44	89.42	6.04
61	bipyr	22.85	5.30	36.51	4.35	38.88	1.99	43.12	4.54
159	tetra	49.23	2.51	54.59	5.19	59.20	6.29	56.44	6.34
14	tetra	45.03	6.95	44.15	2.93	44.89	3.34	51.26	3.88
37	octa	38.68	4.47	43.66	3.76	46.81	6.09	42.20	2.96
1	tetra	41.85	1.53	47.11	2.25	45.47	2.83	49.17	3.01

The symmetric bipyramidal structure 'bypir 14' exhibits smaller values for the bulk modulus, ranging from 70 GPa to 90 GPa and following the previously described ordering across the series. The distorted bipyramidal structure 'bypir 61' exhibits the smaller values for the bulk modulus for Mn, Fe and Co. In the case of the tetrahedral phase, the reported values for the bulk modulus range from 35 GPa to 55 GPa, being therefore smaller by a factor of two than the findings for the octahedral structures. A clear ordering of the values across the series can not be observed. The semi-amorphous 'tetra/bp 170' structure exhibits a similar behaviour.